J. Fluid Mech. (2003), *vol.* 493, *pp.* 181–190.
DOI: 10.1017/S0022112003005731 Printed in the United Kingdom

Evolution of a vortex in a rotating conducting fluid

By F. SISO-NADAL, P. A. DAVIDSON AND W. R. GRAHAM

Department of Engineering, University of Cambridge, Trumpington Street, Cambridge, CB2 1PZ, UK

(Received 1 May 2003 and in revised form 8 July 2003)

In this paper we examine the evolution of an isolated vortex in a rotating conducting fluid which is threaded by a uniform magnetic field. Magnetic and rotation forces dominate over nonlinear and viscous effects and the flow is incompressible. The study is formulated in terms of an unbounded initial value problem with emphasis on the asymptotic solutions at large time. When the homogeneous imposed magnetic field is normal to the rotation axis it is observed that inertial waves, induced by the prescribed initial condition, transport energy on planes perpendicular to the magnetic field to form a series of counter-rotating travelling eddies. Transport along magnetic field lines occurs by pseudo-diffusion, common at low magnetic Reynolds numbers, and by wave propagation from those inertial waves that survive the strong magnetic damping.

1. Introduction

Vortices in magnetostrophic balance tend to evolve into complex structures, since both the Coriolis and Lorentz forces are anisotropic. In this article we study the mechanisms which underlie this complex evolution, and draw conclusions about the general shapes adopted by eddies at large time.

There are many naturally occurring flows which involve rotating conducting fluids, the flow within the core of the Earth being one example. The present work is motivated by the study of motion in the core whose scale ($\sim$ 1–10 km) is much smaller than the characteristic dimension of the terrestrial outer core ($\sim$ 2000 km). Small-scale motion in the core is important for several reasons. For example, it enhances the diffusion of heat and chemical species and plays a key role in classical theories of the geodynamo (i.e. the α-effect). However, numerical simulations of the core cannot resolve these scales and so there is a need to understand better the behaviour of the small scales as a first step towards parameterizing their effect (see Braginsky & Roberts 1995). Near the solid inner core, which is the most likely source of small-scale motion, there is thought to be an intense east–west magnetic field, and so the dominant forces acting on an eddy are the Lorentz and Coriolis forces. Our aim is to clarify the way in which these forces shape and dissipate small-scale motion.

From the numerical values of the parameters relevant to the study of small-scale motion in, for example, Moffatt & Loper (1994), it is assumed here that the Rossby number Ro and the magnetic Reynolds number R_m are small. These regimes, taken separately, have been extensively documented in the literature. Consider first the case where an eddy evolves in a uniform magnetic field B_0. The key dimensionless group is $R_m = ul/\eta$, a Reynolds number based on the magnetic diffusivity η and the relevant velocity and length scales u, l. At low R_m, the Lorentz force causes momentum to

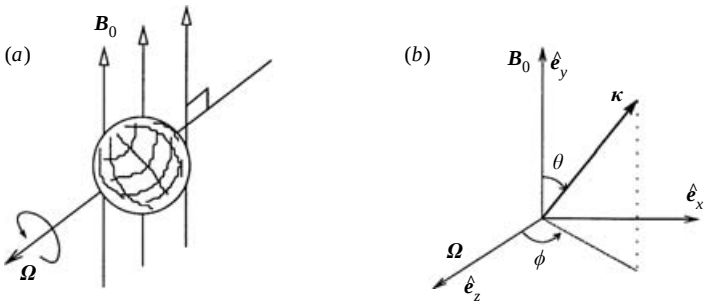

FIGURE 1. (*a*) Vortex threaded by a uniform magnetic field in a rotating fluid. (*b*) Coordinate system defining the wavevector.

diffuse along field lines. Studies by, for instance, Moffatt (1967) and Davidson (1997) have suggested that the characteristic length scale parallel to the magnetic field l_B grows at a rate

$$l_B \sim l_\perp (t/\tau)^{1/2}, \tag{1.1}$$

where $l_\perp$ denotes the perpendicular length scale and

$$\tau = \rho/(\sigma B_0^2) \tag{1.2}$$

is the Joule damping time. Here ρ and σ are the density and the electrical conductivity of the fluid. This diffusion-like mechanism will be here referred to as pseudo-diffusion. The Joule damping time τ plays a second important role at low R_m: it is the characteristic time scale on which a static magnetic field $\boldsymbol{B}_0$ damps out motion (see Shercliff 1965).

The Rossby number is $Ro = u/2\Omega l$ for a background rotational rate Ω. Low Ro characterizes a regime where the nonlinear inertial forces are negligible (cf. Greenspan 1968). In addition, it suggests that the characteristic group velocity of inertial waves, $2\Omega l$, is greater than the characteristic flow velocity, and one expects energy and momentum to be transported primarily by inertial oscillations. Several features of inertial waves have been touched upon by, for example, Bretherton (1967) in the context of the disturbances generated by rigid bodies moving through a rotating fluid. A common feature is the appearance of Taylor columns in which the fluid moves with the body, a feature attributed to the propagation of inertial waves. However, studies of the effects of rotation on deformable bodies for which the velocity is not constantly prescribed, are rare (see Loper 2001) and the aim of the present work is to investigate the combined effects of rotation and a uniform imposed magnetic field on a freely evolving vortex, cf. figure 1(*a*). Of particular importance is that the growth of the vortex along the rotation axis, based on wave propagation, and along the field lines, based on (1.1), is expected to be controlled by different time scales, as discussed previously by Davidson & Siso-Nadal (2002).

2. Formulation

2.1. *The governing equations*

Consider an unbounded rapidly rotating fluid which is threaded by a uniform imposed magnetic field $\boldsymbol{B}_0$. The evolution of the velocity field $\boldsymbol{u}$ is governed by

$$\partial_t \boldsymbol{u} + 2\boldsymbol{\Omega} \times \boldsymbol{u} = -\nabla p + (\mu_0 \rho)^{-1} (\boldsymbol{B}_0 \cdot \nabla)\boldsymbol{b}; \tag{2.1}$$

the last term on the right-hand side is the rotational part of the Lorentz force, $\boldsymbol{b}$ the induced magnetic field and μ_0 the magnetic permeability (cf. Shercliff 1965). The fluid pressure has been augmented by the irrotational part of the Lorentz force and by the centripetal force and both $\boldsymbol{u}$ and $\boldsymbol{b}$ are solenoidal. If R_m is small then Ohm's law reduces to

$$\boldsymbol{j} = \sigma(-\nabla\phi_e + \boldsymbol{u} \times \boldsymbol{B}_0), \tag{2.2}$$

where $\boldsymbol{j}$ is the current density and ϕ_e the electric potential. When combined with Ampère's law, $\nabla \times \boldsymbol{b} = \mu_0 \boldsymbol{j}$, this yields a simplified form of the induction equation,

$$\eta\nabla^2\boldsymbol{b} = -\boldsymbol{B}_0 \cdot \nabla\boldsymbol{u}, \tag{2.3}$$

where $\eta = (\mu_0\sigma)^{-1}$. Substituting (2.3) into the linearized momentum equation (2.1) gives

$$\partial_t\boldsymbol{u} + 2\Omega(\hat{\boldsymbol{e}}_\Omega \times \boldsymbol{u}) = -\nabla p - \tau^{-1}\nabla^{-2}(\hat{\boldsymbol{e}}_B \cdot \nabla)^2\boldsymbol{u}, \tag{2.4}$$

where $\hat{\boldsymbol{e}}_\Omega$ and $\hat{\boldsymbol{e}}_B$ are unit vectors in the directions indicated by their subscripts and ∇^{-2} is the inverse of the Laplacian defined via the Biot-Savart law.

An evolution equation for the vorticity, $\boldsymbol{\omega} = \nabla \times \boldsymbol{u}$, is readily found from the momentum equation. It is (Davidson & Siso-Nadal 2002)

$$[\partial_t + \tau^{-1}\nabla^{-2}(\hat{\boldsymbol{e}}_B \cdot \nabla)^2]^2\nabla^2\boldsymbol{\omega} = -(2\Omega)^2(\hat{\boldsymbol{e}}_\Omega \cdot \nabla)^2\boldsymbol{\omega}, \tag{2.5}$$

an equation which is also obeyed by the velocity field $\boldsymbol{u}$.

2.2. *Inertial waves at low R_m*

Introduce the Fourier transform pair

$$\hat{\boldsymbol{\omega}} = \frac{1}{(2\pi)^3}\int \boldsymbol{\omega}\exp(-\mathrm{i}\boldsymbol{\kappa} \cdot \boldsymbol{x})\,\mathrm{d}^3\boldsymbol{x}, \qquad \boldsymbol{\omega} = \int \hat{\boldsymbol{\omega}}\exp(\mathrm{i}\boldsymbol{\kappa} \cdot \boldsymbol{x})\,\mathrm{d}^3\boldsymbol{\kappa},$$

and transform (2.5) to yield

$$[\mathrm{d}/\mathrm{d}t + \tau^{-1}(\hat{\boldsymbol{e}}_B \cdot \hat{\boldsymbol{e}}_\kappa)^2]^2\ \hat{\boldsymbol{\omega}} = -(2\Omega)^2(\hat{\boldsymbol{e}}_\Omega \cdot \hat{\boldsymbol{e}}_\kappa)^2\hat{\boldsymbol{\omega}}, \tag{2.6}$$

the general solution of which is

$$\hat{\boldsymbol{\omega}} = \exp[-(\hat{\boldsymbol{e}}_B \cdot \hat{\boldsymbol{e}}_\kappa)^2 t/\tau]\{\boldsymbol{A}\exp[-\mathrm{i}2\Omega(\hat{\boldsymbol{e}}_\Omega \cdot \hat{\boldsymbol{e}}_\kappa)t] + \boldsymbol{B}\exp[\mathrm{i}2\Omega(\hat{\boldsymbol{e}}_\Omega \cdot \hat{\boldsymbol{e}}_\kappa)t]\}. \tag{2.7}$$

Here $\boldsymbol{A}$ and $\boldsymbol{B}$ depend on the initial conditions and $\hat{\boldsymbol{e}}_\kappa$ is a unit vector in the direction of the wavevector $\boldsymbol{\kappa}$. The inversion of (2.7) yields the vorticity as a superposition of plane waves,

$$\boldsymbol{\omega} = \int \boldsymbol{A}\exp[\mathrm{i}(\boldsymbol{\kappa} \cdot \boldsymbol{x} - \lambda t)]\,\mathrm{d}^3\boldsymbol{\kappa} + \int \boldsymbol{B}\exp[\mathrm{i}(\boldsymbol{\kappa} \cdot \boldsymbol{x} + \lambda^* t)]\,\mathrm{d}^3\boldsymbol{\kappa}, \tag{2.8}$$

where

$$\lambda = 2\Omega(\hat{\boldsymbol{e}}_\Omega \cdot \hat{\boldsymbol{e}}_\kappa) - \mathrm{i}\tau^{-1}(\hat{\boldsymbol{e}}_B \cdot \hat{\boldsymbol{e}}_\kappa)^2 \tag{2.9}$$

is the complex frequency and the star denotes a complex conjugate. In the dispersion relation (2.9) the real term represents the frequency of inertial waves and the imaginary part indicates that motion is damped by Joule dissipation. The characteristics of these waves can perhaps be seen clearly by examination of the velocity field due to a single Fourier component. The velocity of the modified waves is found explicitly from the curl of the momentum equation (2.4), and one finds that

$$\boldsymbol{u} = U[\hat{\boldsymbol{e}}_\zeta\cos\varpi \pm (\hat{\boldsymbol{e}}_\kappa \times \hat{\boldsymbol{e}}_\zeta)\sin\varpi]\exp[-(\hat{\boldsymbol{e}}_B \cdot \hat{\boldsymbol{e}}_\kappa)^2 t/\tau]. \tag{2.10}$$

Here $\hat{\boldsymbol{e}}_\zeta$ is a vector perpendicular to the direction of wave propagation $\hat{\boldsymbol{e}}_\kappa$, U is a constant and $\varpi = \boldsymbol{\kappa}\cdot\boldsymbol{x} - \mathrm{Re}(\lambda)t$. Note that, as for any incompressible flow, $\boldsymbol{u}$ is normal to $\hat{\boldsymbol{e}}_\kappa$. Furthermore, the trajectories are circular. This expression is the same as the trajectory equation for inertial waves in a non-conducting fluid given by Phillips (1977), except for the appearance of the damping term.

The current and electric potential associated with the oscillations can be found from the curl and divergence (respectively) of Ohm's law (2.2). We note that, when $\boldsymbol{\kappa}$ is parallel to $\boldsymbol{B}_0$, the potential is zero and the Lorentz force is antiparallel to $\boldsymbol{u}$, resulting in magnetic damping. However, when $\boldsymbol{\kappa}$ is perpendicular to the field, the electrical potential balances the term $\boldsymbol{u}\times\boldsymbol{B}_0$, the Lorentz force is zero and the wave is devoid of damping (see also Moffatt 1970). The same conclusions concerning dissipation can be reached by examining the exponential in (2.10), from which one finds the following dissipation condition:

$$\hat{\boldsymbol{e}}_B\cdot\hat{\boldsymbol{e}}_\kappa \sim (t/\tau)^{-1/2}. \tag{2.11}$$

Wave motion associated with a particular wave component $\boldsymbol{\kappa}$ decays on a time scale

$$t/\tau \sim (\hat{\boldsymbol{e}}_B\cdot\hat{\boldsymbol{e}}_\kappa)^{-2}. \tag{2.12}$$

The magnetic field continuously dissipates waves, starting with those with wavevector $\boldsymbol{\kappa}$ parallel to $\boldsymbol{B}_0$ and proceeding to those which are nearly aligned to the field. Clearly, the longest surviving waves propagate at right angles to the magnetic field, i.e. $\hat{\boldsymbol{e}}_\kappa\cdot\hat{\boldsymbol{e}}_B \sim 0$.

The transport of energy by inertial waves is characterized by the group velocity

$$\boldsymbol{C}_g = 2\Omega|\boldsymbol{\kappa}|^{-1}\,[\hat{\boldsymbol{e}}_\Omega - \hat{\boldsymbol{e}}_\kappa(\hat{\boldsymbol{e}}_\Omega\cdot\hat{\boldsymbol{e}}_\kappa)], \tag{2.13}$$

and it follows that

$$(\hat{\boldsymbol{e}}_\kappa\times\hat{\boldsymbol{e}}_\Omega)\cdot\boldsymbol{C}_g = 0. \tag{2.14}$$

This equation states that the energy associated with a wavevector $\hat{\boldsymbol{e}}_\kappa$ is always confined to planes spanned by $\hat{\boldsymbol{e}}_\kappa$ and the axis of rotation, which is relevant to the analysis in the next section.

3. Asymptotic solutions

A more tractable form for $\boldsymbol{\omega}$, valid for large time, is now derived. Let the orientation of the imposed vectors be such that $\boldsymbol{B}_0 = \langle 0, B_0, 0\rangle$ and $\boldsymbol{\Omega} = \langle 0, 0, \Omega\rangle$ in a Cartesian frame (x, y, z). The relative importance of magnetic to Coriolis forces is measured by the Elsasser number which, in terms of the relevant time scales, is

$$\Lambda = (2\Omega\tau)^{-1}. \tag{3.1}$$

Of particular importance for the study of the dynamics of the Earth's core is the case for which $\Lambda = O(1)$. Time could be scaled by either Ω^{-1} or τ and the scaling

$$\mathfrak{t} = 2\Omega t \tag{3.2}$$

is introduced.

Attention is restricted to waves with phase speed components in the positive z-direction, i.e. to the first integral in (2.8). The ith component of this integral, say ω_i^+, is now analysed in detail. It is convenient to transform the wavevector $\boldsymbol{\kappa}$ to spherical polar coordinates (κ, θ, ϕ) as shown in figure 1(*b*) with ϕ being the azimuthal angle

measured from the z-axis about the y-axis, θ being the co-latitude and $\kappa = |\boldsymbol{\kappa}|$. Then

$$\omega_i^+ = \int \mathrm{d}\theta \exp(-\mathrm{t}\Lambda \cos^2\theta) \sin\theta \int A_i \kappa^2 \exp(\mathrm{i}\mathrm{t}h)\, \mathrm{d}\phi\, \mathrm{d}\kappa, \tag{3.3}$$

where

$$h = [\kappa x \sin\phi + (\kappa z - 1)\cos\phi] \sin\theta + \kappa y \cos\theta. \tag{3.4}$$

The coordinates (x, y, z) appearing in this phase function are scaled forms of the original variables (x, y, z), i.e.

$$\{x, y, z\} = \{x/2\Omega t,\ y/2\Omega t,\ z/2\Omega t\}. \tag{3.5}$$

This scaling allows the coordinate system to 'follow' the propagation of the inertial waves expected in this problem.

The behaviour of (3.3) at large times is now examined. It is assumed that $\mathrm{t} \gg 1$ while $\Lambda = O(1)$ so that time is larger than both the rotation period and the magnetic damping time, i.e. $2\Omega t \gg 1$ and $t/\tau \gg 1$. The asymptotic estimation of such integrals is well documented; see, for instance, Bleistein & Handelsman (1986) or Wong (1989). The resulting asymptotic series depends on the local behaviour of the integrand at a critical point, which represents a dominant wavevector $\boldsymbol{\kappa}_c$. In (3.3), the argument of the exponential in the inner integral is purely imaginary, and a multidimensional stationary phase method is called for. The critical points are identified from $\partial_\kappa h = \partial_\phi h = 0$. These equations do not admit an explicit solution for all y, but for $y \ll z, x$ one finds

$$\kappa_c = \frac{z}{r^2} \mp \left(\frac{x}{r}\cot\theta\right)\frac{y}{r} + O\left(\frac{y^2}{r^2}\right), \tag{3.6a}$$

$$\cos\phi_c = \mp\frac{x}{r} - \left(\frac{z}{r}\cot\theta\right)\frac{y}{r} + O\left(\frac{y^2}{r^2}\right), \tag{3.6b}$$

where $r^2 = x^2 + z^2$. Our interest in regions for which $y \ll r$ is motivated from the following. The anisotropic damping specified by (2.11) results in a confinement of wavevectors to planes perpendicular to $\boldsymbol{B}_0$. In the present configuration, these perpendicular planes are parallel to $\hat{\boldsymbol{e}}_\Omega$ and it follows from (2.14) that the group velocity, quickly transporting energy at a rate Ω, is predominantly coplanar to these perpendicular (x, z)-planes.

The details of the application of the stationary phase method to the inner integral in (3.3) are shown in the Appendix and the resultant expression renders ω_i^+ into

$$\omega_i^+ = \frac{2\pi}{\mathrm{t}} \int \frac{A_i(\phi_c, \kappa_c, \theta)\kappa_c^2}{|x\cos\phi_c - z\sin\phi_c|} \exp(\mathrm{t}f)\, \mathrm{d}\theta, \tag{3.7}$$

where

$$f = -\Lambda\cos^2\theta - \mathrm{i}\cos\phi_c \sin\theta. \tag{3.8}$$

This integral can be estimated via the method of steepest descents. The critical value of θ is found from $\partial_\theta f = 0$, and it is

$$\theta_c = \frac{\pi}{2} - \frac{z}{r}\left(\frac{\pm x/r + \mathrm{i}2\Lambda}{x^2/r^2 + 4\Lambda^2}\right)\frac{y}{r} + O\left(\frac{y^3}{r^3}\right), \tag{3.9}$$

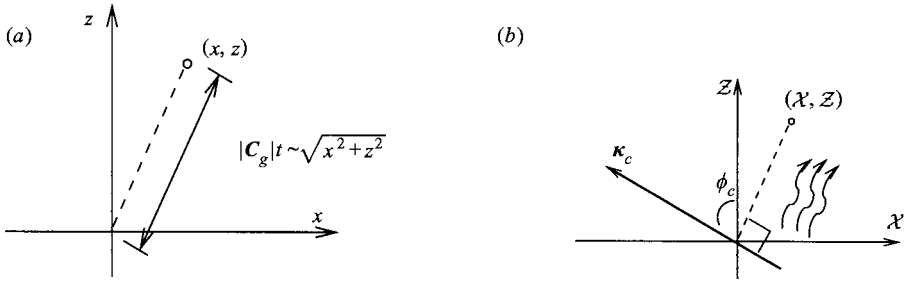

FIGURE 2. Interpretation of the dominant wavevector. (*a*) The magnitude of the dominant wavevector is such that energy is found at the point of interest. (*b*) Dominant waves propagate at right angles to the vector $\langle \mathcal{x}, \mathcal{z} \rangle$.

The integral in (3.7) is now evaluated about this critical point. The details are shown in the Appendix and the resulting expression is

$$\omega_i^+ \sim \frac{A_i^c z^2}{\mathrm{t}(\Lambda \mathrm{t})^{1/2}} \left(\frac{\pi^3}{a}\right)^{1/2} \frac{2}{r^5} \exp(\mathrm{t} f_c) \exp\left[\mathrm{i}\frac{1}{2}\tan^{-1}\left(\frac{\lambda_\Omega}{2\Lambda}\right)\right]. \tag{3.10}$$

Here

$$f_c \sim -\frac{1}{\Lambda}\left(\frac{z}{2ar}\right)^2\left(\frac{y}{r}\right)^2 - \mathrm{i}\lambda_\Omega\left[1+\frac{1}{2}\left(\frac{z}{2ar}\right)^2\left(\frac{y}{r}\right)^2\right] \tag{3.11}$$

and

$$a^2 = \left(\frac{\lambda_\Omega}{2\Lambda}\right)^2 + 1, \quad \lambda_\Omega = \mp\frac{x}{r}. \tag{3.12}$$

The term λ_Ω is the first term in expansion (3.6*b*) and thus $2\Omega\lambda_\Omega$ represents the frequency of the critical waves. Also $A_i^c = A_i(\boldsymbol{\kappa_c})$. To obtain (3.10), terms up to order $(y/r)^2$ have been retained.

The critical value of the wavevector $\boldsymbol{\kappa}_c = \langle \kappa_c, \phi_c, \theta_c \rangle$, as specified by (3.6) and (3.9) is interpreted in what follows. First, the critical angle θ_c between the wavevector and $\boldsymbol{B}_0$ is analysed. The values of y corresponding to significant motions follow from the real part of the exponential in (3.10): $y/r \sim (2ar/z)(\Lambda/\mathrm{t})^{1/2}$. Thus (3.9) suggests that, as time advances, the dominant wavevectors approach perpendicularity to the field lines at a rate of $O[(t/\tau)^{-1/2}]$. This is in accordance with (2.11) and implies that, for sufficiently large times, energy is confined predominantly to planes perpendicular to the field lines.

The magnitude of the critical wavevector, as given in (3.6*a*), indicates that the distance travelled by the associated energy along (x, z)-planes (perpendicular to $\boldsymbol{B}_0$) is approximately equal to the distance from the origin to the point of interest (x, z). For, the distance travelled by the energy, $|\boldsymbol{C}_g|t$, can be written as

$$|\boldsymbol{C}_g|t \sim 2\Omega t|\sin\phi_c|/\kappa_c \sim 2\Omega t z/\kappa_c r, \tag{3.13}$$

so that the substitution of κ_c into the previous expression gives

$$|\boldsymbol{C}_g|t \sim (x^2+z^2)^{1/2}. \tag{3.14}$$

This idea is depicted in figure 2(*a*).

The direction of propagation of the dominant wavevector is inferred from ϕ_c, as given in (3.6*b*). It indicates that the critical wavevector advances preferentially at

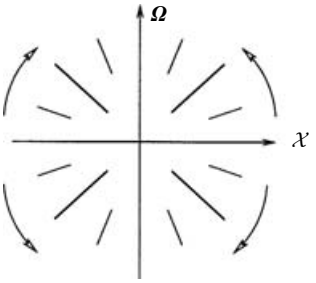

FIGURE 3. Lines of constant phase.

right angles to the position vector $\langle x, z\rangle$; cf. figure 2(*b*). This suggests that the critical waves radiate like pure inertial waves, at right angles to $\boldsymbol{\kappa}$.

There is one more piece of information one can obtain from the critical point. It follows from (3.6*a*) that only positive z values contribute to ω_i^+. Since this integral represents waves with phase speed components in the positive z-direction, the $\hat{\boldsymbol{e}}_\Omega$ component of both the phase velocity and the velocity at which energy propagates have the same sign. This is consistent with the behaviour of inertial waves (see Lighthill 1978, Epilogue).

The exponential term in (3.10) possesses some interesting features which will be now discussed. Consider first the leading imaginary argument,

$$\exp(-\mathrm{i}t\lambda_\Omega) = \exp[\pm\mathrm{i}tx(x^2+z^2)^{-1/2}], \tag{3.15}$$

which is independent of y. For a given time, lines of constant phase are lines for which $z/x =$ constant. As time advances, the lines of constant phase rotate towards being aligned with the axis of rotation, giving rise to new peaks or troughs which appear at lateral planes as shown in the sketch of figure 3. This behaviour is a common propagation of inertial waves and was discussed by Bretherton (1967, figure 4) in the context of two-dimensional motion. Thus the oscillatory patterns resemble two-dimensional inertial wave propagation in non-conducting fluids.

Now, with reference to the flow evolution along field lines, consider the real exponential argument in (3.10) which represents a decay of motion along field lines. The characteristic length scale along this direction is

$$y \sim \frac{2ar^2}{z}\left(\frac{t}{\tau}\right)^{1/2} \sim \frac{2a}{\kappa_c}\left(\frac{t}{\tau}\right)^{1/2}, \tag{3.16}$$

a scaling valid for regions around the wave front $r/l = O(1)$. As we shall see, there are two mechanisms whereby energy is transported along field lines: pseudo-diffusion and propagation by waves whose wavevectors have non-zero components in the $\boldsymbol{B}_0$-direction. In the one hand, when magnetic effects dominate (large Λ), the dissipation of waves is strong and the only surviving wavevectors are those that propagate at right angles to $\boldsymbol{B}_0$. These waves redistribute energy on the perpendicular planes exclusively and this energy is instantaneously channelled along $\boldsymbol{B}_0$ by pseudo-diffusion. By instantaneous we mean that the characteristic magnetic time τ is smaller than the period of the oscillations. It follows from (3.16) that when Λ is large and $|\lambda_\Omega|/\Lambda \ll 1$, that is when $a \sim 1$,

$$y \sim \frac{2}{\kappa_c}\left(\frac{t}{\tau}\right)^{1/2}. \tag{3.17}$$

This scaling characterizes pseudo-diffusion as written in (1.1). Note that κ_c^{-1} represents the characteristic length scale on the perpendicular plane and so it plays the same role as $l_\perp$ in (1.1).

On the other hand, when magnetic effects are weak, another means of transport along field lines prevails: wave propagation. When the field strength is weak, dissipation of waves occurs slowly in the sense that the magnetic damping time τ is larger than the period of oscillation. Under these circumstances, it is possible to find waves whose wavevectors $\boldsymbol{\kappa}$ are not perpendicular to the field lines, although as time advances, those wavevectors with largest $\hat{\boldsymbol{e}}_B$ components are lost at a rate given by (2.12). The group velocity of the non-perpendicular waves is such that energy is transported along the magnetic axis. In this weak field scenario, the characteristic length scale along the field lines is found by taking $|\lambda_\Omega|/\Lambda \gg 1$ in (3.16) giving

$$y \sim \frac{|\lambda_\Omega|}{\Lambda \kappa_c} \left(\frac{t}{\tau}\right)^{1/2}. \tag{3.18}$$

That expression (3.18) is associated with wave transport can be seen as follows. The distance travelled by the energy along the $\boldsymbol{B}_0$-axis is

$$(\boldsymbol{C}_g \cdot \hat{\boldsymbol{e}}_B)t = -2\Omega t |\boldsymbol{\kappa}|^{-1} (\hat{\boldsymbol{e}}_\kappa \cdot \hat{\boldsymbol{e}}_\Omega)(\hat{\boldsymbol{e}}_\kappa \cdot \hat{\boldsymbol{e}}_B). \tag{3.19}$$

The inner product $\hat{\boldsymbol{e}}_\kappa \cdot \hat{\boldsymbol{e}}_\Omega = \cos\phi \sin\theta$ and can, for large time, be approximated as $|\lambda_\Omega|$, cf. (3.6*b*), (3.9) and (3.12). Also $(\hat{\boldsymbol{e}}_\kappa \cdot \hat{\boldsymbol{e}}_B) \sim \pm(t/\tau)^{-1/2}$ from (2.11). The substitution of these expressions into (3.19) results, in accordance with (3.18), in

$$(\boldsymbol{C}_g \cdot \hat{\boldsymbol{e}}_B)t \sim \pm \frac{|\lambda_\Omega|}{\Lambda |\boldsymbol{\kappa}|} \left(\frac{t}{\tau}\right)^{1/2}. \tag{3.20}$$

Any oscillations along the y-axis come from the third term in (3.11), which displays a stationary point at $y = 0$. The width of this stationary phase point is of the same order as the characteristic length scale along the magnetic field lines, suggesting that there are no oscillations of practical importance in this direction.

Finally, from the two contributions of (3.10), one finds that (cf. the Appendix)

$$\omega_i^+ \sim \frac{|A_i|^c z^2}{\mathrm{t}(\Lambda \mathrm{t})^{1/2}} \left(\frac{\pi^3}{a}\right)^{1/2} \frac{4}{r^5} \exp\left[-\left(\frac{z}{2ar}\right)^2 \left(\frac{\mathrm{t}}{\Lambda}\frac{y^2}{r^2}\right)\right] \cos(-\mathrm{t}|\lambda_\Omega| + \beta + \alpha_i), \tag{3.21}$$

where $|A_i|^c$ and α_i are the modulus and phase of A_i^c and

$$\beta = \frac{1}{2}\tan^{-1}\left(\frac{|\lambda_\Omega|}{2\Lambda}\right) - |\lambda_\Omega| \left(\frac{z}{2ar}\right)^2 \left(\frac{\mathrm{t}}{2}\frac{y^2}{r^2}\right). \tag{3.22}$$

The algebraic time decay shown in (3.21) is representative. Decays of order $\mathrm{t}^{-3/2}$ are common in energy-preserving three-dimensional wave propagation, where waves propagate along each axis at a rate Ω. On the other hand, the present problem is quite different: growth along $\boldsymbol{B}_0$ happens at a slower rate, which implies that energy is not conserved.

4. Example and discussion

The asymptotic expressions presented in the previous section are generic, in the sense that they are not specific to a particular initial condition. Nevertheless, it is useful to prescribe an initial flow and follow its development.

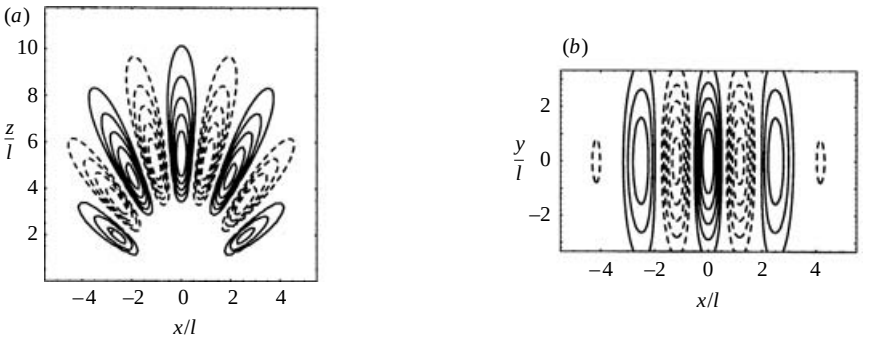

FIGURE 4. Contours of vorticity ω_z when $\mathrm{t} = 5\pi$ for a vortex initially aligned with $\boldsymbol{\Omega}$. $(a)y/l = 1.5; (b)z/l = 6$. Dashed contours represent negative vorticity and $\Lambda = 1$.

The constants of integration in (2.8) are found by specifying an initial vorticity field, say $\boldsymbol{\omega}_0$. The initial rate of change of $\boldsymbol{\omega}_0$ is set by the curl of (2.4), whose transform is

$$\partial_t \hat{\boldsymbol{\omega}}_0 = -\tau^{-1}(\hat{\boldsymbol{e}}_B \cdot \hat{\boldsymbol{e}}_\kappa)^2 \hat{\boldsymbol{\omega}}_0 - \mathrm{i}2\Omega|\boldsymbol{\kappa}|(\hat{\boldsymbol{e}}_\Omega \cdot \hat{\boldsymbol{e}}_\kappa)\hat{\boldsymbol{u}}_0, \tag{4.1}$$

so that the ith component of $\boldsymbol{A}$ becomes

$$A_i = \tfrac{1}{2}(\hat{\omega}_0 + |\boldsymbol{\kappa}|\hat{u}_0)_i. \tag{4.2}$$

Consider an axisymmetric spherical Gaussian vortex aligned with the rotation axis (z-direction). The initial velocity is

$$\boldsymbol{u}_0 = \gamma(\hat{\boldsymbol{e}}_z \times \boldsymbol{x}) \exp(-|\boldsymbol{x}|^2/l^2), \tag{4.3}$$

where γ is a measure of the angular velocity of the vortex and l is the characteristic size of the initial disturbance. The transformed velocity and vorticity are

$$\hat{\boldsymbol{u}}_0 = -\mathrm{i}\mathcal{D}(\hat{\boldsymbol{e}}_z \times \hat{\boldsymbol{e}}_\kappa), \qquad (\hat{\omega}_0)_i = \mathfrak{D}(\delta_{3i} - \kappa_3\kappa_i|\boldsymbol{\kappa}|^{-2}), \tag{4.4}$$

where $\mathcal{D} = (16\pi^{3/2})^{-1}\gamma l^5|\boldsymbol{\kappa}| \exp(-|\boldsymbol{\kappa}|^2 l^2/4)$ and $\mathfrak{D} = (16\pi^{3/2})^{-1}\gamma l^5|\boldsymbol{\kappa}|^2 \exp(-|\boldsymbol{\kappa}|^2 l^2/4)$. In (4.4), δ_{ji} is the Kronecker delta and the index 3 represents the z-direction.

We can now study the evolution of a vortex as written in (4.3). Considering the z-component of (3.21), the modulus and phase of A_z are, from (4.2), (4.4) and (3.9)

$$|A_z|^c \sim \tfrac{1}{2}\mathfrak{D}(\kappa_c)\sin^2\phi_c, \quad \alpha_z = 0. \tag{4.5}$$

The substitution of A_z and α_z into (3.21) gives the contours of ω_z shown in figure 4. Figure 4(a) shows the vorticity on a plane perpendicular to the magnetic field. It is seen that the vortex, which is originally situated at the origin, evolves into a series of counter-rotating eddies. Each of these vortical structures follows the behaviour of the lines of constant phase as depicted in figure 3 and, as waves propagate, a substantial amount of energy leaks away from the axis of rotation. The vorticity is concentrated in packets which detach themselves from the origin and travel away from it. Both the speed at which the packets travel and their rate of stretch scale with $2\Omega t$.

Figure 4(b) shows ω_z on a plane parallel to the magnetic field, and reiterates the fact that the flow along field lines is devoid of oscillations. The vortical patterns in planes perpendicular to the field lines (where waves are free to propagate) are extruded in the direction of the applied magnetic field by a combination of the two transport mechanisms mentioned in § 3.

The authors would like to thank John Lister and Nigel Peake for fruitful discussions.

Appendix. Mathematical details

The inner integral in (3.3) was approximated using a multidimensional stationary phase method as documented by Bleistein & Handelsman (1986, § 8.4), giving

$$\int g(\boldsymbol{x})\exp[\mathrm{i}\mathfrak{t}h(\boldsymbol{x})]\,\mathrm{d}^2\boldsymbol{x} \sim \left(\frac{2\pi}{\mathfrak{t}}\right) g(\boldsymbol{x}_c)\big|\det\left(H^c_{ij}\right)\big|^{-1/2}\exp\left[\mathrm{i}\mathfrak{t}h(\boldsymbol{x_c})+\frac{\mathrm{i}\pi\mathrm{sig}\left(H^c_{ij}\right)}{4}\right], \quad (A\,1)$$

where H^c_{ij} is the Hessian matrix evaluated at the critical point (3.6) and sig$(\cdot)$ is its signature (the number of positive eigenvalues minus the number of negative eigenvalues). For the present problem, $\det(H^c_{ij}) = -(x\cos\phi_c - z\sin\phi_c)^2\sin^2\theta$ and $\mathrm{sig}(H^c_{ij}) = 0$. The inner integral in (3.3) becomes

$$\int A_i\kappa^2\exp(\mathrm{i}\mathfrak{t}h)\,\mathrm{d}\phi\,\mathrm{d}\kappa \sim \frac{2\pi A_i(\kappa_c,\phi_c,\theta)\kappa_c^2}{\mathfrak{t}|(x\cos\phi_c - z\sin\phi_c)\sin\theta|}\exp[\mathrm{i}\mathfrak{t}h(\kappa_c,\phi_c,\theta)]. \quad (A\,2)$$

This leads to (3.7), where the exponential has a complex argument. A steepest descents method is called for, the relevant formula being (Bleistein & Handelsman 1986, § 7.2)

$$\int g(\theta)\exp[\mathfrak{t}f(\theta)]\,\mathrm{d}\theta \sim \sqrt{\frac{2\pi}{\mathfrak{t}|f''(\theta_c)|}}\,g(\theta_c)\exp[\mathfrak{t}f(\theta_c)]\exp\left\{\mathrm{i}\left[\frac{\pi}{2}-\frac{\arg[f''(\theta_c)]}{2}\right]\right\}. \quad (A\,3)$$

The relevant components at the critical point are

$$|f''(\theta_c)| \sim \left(\lambda_\Omega^2 + 4\Lambda^2\right)^{1/2}, \quad (A\,4)$$

$$\arg\{f''(\theta_c)\} \sim -\tan^{-1}(\lambda_\Omega/2\Lambda) + \pi. \quad (A\,5)$$

Substitution of these expressions into (A 3) leads to (3.10), which represents two contributions to ω_i^+. Adding the two contributions leads to (3.21).

REFERENCES

Bleistein, N. & Handelsman, R. A. 1986 *Asymptotic Expansions of Integrals*. Dover.

Braginsky, S. I. & Roberts, P. H. 1995 Equations governing convection in the Earth's core and the geodynamo. *Geophys. Astrophys. Fluid Dyn.* **79**, 1–97.

Bretherton, F. P. 1967 The time-dependend motion due to a cylinder moving in an unbounded rotating or stratified fluid. *J. Fluid Mech.* **28**, 545–70.

Davidson, P. A. 1997 The role of angular momentum in the magnetic damping of turbulence. *J. Fluid Mech.* **336**, 123–50.

Davidson, P. A. & Siso-Nadal, F. 2002 On the structure of small-scale motion in the core of the Earth. *Geophys. Astrophys. Fluid Dyn.* **96**, 49–76.

Greenspan, H. P. 1968 *The Theory of Rotating Fluids*. Cambridge University Press.

Lighthill, M. J. 1978 *Waves in Fluids*. Cambridge University Press.

Loper, D. E. 2001 On the structure of a Taylor column driven by a buoyant parcel in an unbounded rotating fluid. *J. Fluid Mech.* **427**, 131–65.

Moffatt, H. K. 1967 On the supression of turbulence by a uniform magnetic field. *J. Fluid Mech.* **28**, 571–92.

Moffatt, H. K. 1970 Dynamo action associated with random inertial waves in a rotating conducting fluid. *J. Fluid Mech.* **44**, 705–19.

Moffatt, H. K. & Loper, D. E. 1994 The magnetostrophic rise of a bouyant parcel in the Earth's core. *Geophys. J. Intl* **117**, 394–402.

Phillips, O. M. 1977 *The Dynamics of the Upper Ocean*. Cambridge University Press.

Shercliff, J. A. 1965 *A Textbook of Magnetohydrodynamics*. Pergamon.

Wong, R. 1989 *Asymptotic Approximations of Integrals*. Academic.